

DRAFT VERSION MAY 21, 2024

Typeset using L^AT_EX preprint style in AASTeX631

Strong magnetic field inside degenerate relativistic plasma and the impacts on the neutrino transport in Core-Collapse Supernovae

YUDONG LUO,^{1,2} SHUAI ZHA,^{3,4,5} AND TOSHITAKA KAJINO^{6,7,8}

¹*School of Physics, Peking University, Beijing 100871, China*

²*Kavli Institute for Astronomy and Astrophysics, Peking University, Beijing 100871, China*

³*Yunnan Observatories, Chinese Academy of Sciences (CAS), Kunming 650216, China*

⁴*Key Laboratory for the Structure and Evolution of Celestial Objects, CAS, Kunming 650216, China*

⁵*International Centre of Supernovae, Yunnan Key Laboratory, Kunming 650216, China*

⁶*School of Physics, Peng Huanwu Collaborative Center for Research and Education, and International Research Center for Big-Bang Cosmology and Element Genesis, Beihang University, Beijing 100191, China*

⁷*Graduate School of Science, The University of Tokyo, Tokyo 113-0033, Japan*

⁸*National Astronomical Observatory of Japan, Tokyo 181-8588, Japan*

(Received XXX; Revised XXX; Accepted XXX)

Submitted to ApJ

ABSTRACT

We study the impacts of magnetic field on the neutrino transport inside core-collapse supernovae (CCSNe). Magnetic field quantizes the momentum of electrons and positrons, resulting in the modification of weak-interaction cross sections and the chemical potentials of electrons and positrons. We include these changes in the leakage scheme of neutrino transport and perform 1D CCSN simulations with GR1D, assuming the postbounce magnetic field strength of 10^{16-17} G. The results show that the neutrino opacities are enhanced due to the amplified interaction rates, resulting in a larger neutrinosphere. This further reduces the peak value of neutrino luminosities and their decay rates since neutrinos stay longer inside the neutrinosphere. Meanwhile, the neutrino mean energies are smaller shortly after bounce and reach their peak values at later times. As these neutrino properties are crucial in subsequent nucleosynthesis processes, including the νp -process, ν -process, and r -process, our findings suggest that the magnetic field may leave discernible marks on the abundance pattern of nucleosynthesis in CCSN.

Corresponding author: Yudong Luo

yudong.luo@pku.edu.cn

zhashuai@ynao.ac.cn

kajino@buaa.edu.cn

Keywords: Neutrinos transport, Core-Collapse Supernova, Magnetic field

1. INTRODUCTION

Core-collapse supernovae (CCSNe) are one of the major astronomical neutrino sources since the collapse of the iron core of massive stars releases gravitational energy of $\sim 10^{53}$ ergs and neutrinos carry away most of this energy (Bethe 1990). This explosive scenario has been confirmed by the detection of about two dozen neutrino events from SN1987A occurring in the Large Magellanic Cloud, with several Cherenkov detectors, including Kamiokande (Hirata et al. 1987), Irvine–Michigan–Brookhaven detectors (Bionta et al. 1987), and the Mont Blanc Underground Neutrino Observatory (Aglietta et al. 1987).

Although CCSNe are frequently observed, modeling their explosions is challenging since all the known interactions are involved in a complex and physically diverse system. In the commonly accepted explosion mechanism, neutrino transport plays the most essential role: After forming a homologous core, the density keeps increasing, making the core exceed the nuclear matter density ($\sim 2.7 \times 10^{14}$ g cm $^{-3}$, see e.g., Oertel et al. 2017). Then, the core could form a spring-like bounce, and such “oscillation” triggers a shock wave at the core surface. Although the shock tries to traverse the overburdening material, it quickly loses energy via dissociating the infalling matter and emitting neutrinos, and turns into an accretion shock. This shock stalls at $\sim 100 - 200$ km, just above the so-called “gain region”, where the competition between neutrino heating and accretion onto the proto-neutron star (PNS) occurs. Finally, if neutrino heating wins the competition, it leads to the shock revival and eventually a successful explosion (Bethe 1990; Woosley et al. 2002; Janka et al. 2007). Otherwise, the PNS continues contraction and collapses into a black hole if the shock revival fails (see e.g., Sumiyoshi et al. 2006; O’Connor & Ott 2011).

The numerical description of such a “delayed neutrino heating” after initial expansion seldomly realizes self-consistently explosion in a 1D simulation assuming spherical symmetry, except for the lowest-mass progenitors (Kitaura et al. 2006; Fischer et al. 2010; Radice et al. 2017). The success of the delayed supernova mechanism turned out to be sensitive to many aspects such as the mass density structure of the unstable core, the efficiency of energy deposition in the gain region, and the turbulence in the gain region. The consideration of these effects requires realistic multidimensional simulations (see Janka 2017 and references therein).

Neutrinos are both essential in the explosion dynamics and crucial for nucleosynthesis. The neutrino transport during the post-bounce phase determines the electron fraction (Y_e) of the ejecta, which is the key parameter for nucleosynthesis in the later phase, especially for the rapid neutron-capture process (Woosley et al. 1994; Nishimura et al. 2015). The emitted neutrinos from the neutrinosphere can further affect nucleosynthesis via the neutrino-nucleus reactions, i.e., ν -process and ν p-process (Woosley et al. 1990; Frohlich et al. 2006; Wanajo 2006). The neutrino luminosities and spectra at the neutrinosphere are critical inputs for the nucleosynthesis calculation, and those parameters are obtained from the neutrino transport during explosion (Wanajo et al. 2011; Balasi et al. 2015). Moreover, neutrino oscillation could generate a non-Fermi-Dirac spectrum due to the neutrino flavor changes (Mikheev & Smirnov 1986; Langacker et al. 1987; Valle 1987; Roulet 1991). Several nuclei are considered as the main products from ν -process such as ^7Li , ^{11}B , ^{19}F , ^{98}Tc , ^{138}La , ^{180}Ta (Woosley et al. 1990; Heger et al. 2005; Yoshida et al. 2008; Kajino et al. 2014; Travaglio et al. 2018; Hayakawa

et al. 2018; Arcones & Thielemann 2023), which cannot be produced via standard CCSN nucleosynthesis. Therefore, if the abundance of those elements could be determined precisely, one can well constrain neutrino properties such as the mass hierarchy (Sasaki et al. 2017; Kusakabe et al. 2019; Sasaki et al. 2020; Ko et al. 2020; Ko et al. 2022).

Meanwhile, a new-born PNS can contain magnetic field up to 10^{15-17} G (Nakamura et al. 2015; Kiuchi et al. 2015, 2014; Takiwaki et al. 2009; Price & Rosswog 2006; Ruiz et al. 2020; Mösta et al. 2015; Raynaud et al. 2020; Obergaulinger & Aloy 2021; Mösta et al. 2014; Powell et al. 2023). Such a strong magnetic field can affect the neutrino transport because it is governed by weak interactions involving e^\pm . Few studies focused on the impacts of magnetic field on microscopic process and the accompanying impacts on astrophysical sites: Lai & Shapiro (1991); Chakrabarty (1996); Chakrabarty et al. (1997) studied the equation of state (EOS) under a strong magnetic field, Famiano et al. (2020) calculated the r -process nucleosynthesis considering impacts of a strong magnetic field on beta decay and electron-positron capture rates, and Maruyama et al. (2022); Famiano et al. (2022) calculated the neutron star cooling under a strong magnetic field. For a strong magnetic field, e^\pm energy spectrum is quantized, and such an effect could change the neutrino-nucleus cross section, further affecting neutrino opacity and other physical properties.

This work systematically investigates two main impacts of magnetic field on neutrino transport: 1) Magnetic field could affect the motion of electrons and positrons inside the plasma, resulting in electron momentum transverse to the field direction is quantized into Landau levels, then the cross section of weak interaction is modified; 2) The thermodynamic properties of e^\pm strongly rely on their chemical potential μ_e , which also deviates from a field-free case due to the quantization. It is also worth mentioning that several previous studies investigated the neutrino-nucleon interactions inside the magnetic field of PNS (Duan & Qian 2004; Lai & Qian 1998; Arras & Lai 1999) while none of them investigated the effects in CCSN dynamical simulations. Therefore, in this work, we study the neutrino transport inside a magnetic field to self-consistently calculate neutrino properties in CCSN, including luminosity, neutrinosphere radius, and neutrino mean energy.

This paper is arranged as follows. We explain the impacts of magnetic field on weak interactions in Section 2. In Section 3, we first describe the leakage scheme for neutrino transport and the corresponding adaption for the presence of a strong magnetic field. Then, we present the numerical results of CCSN simulations and the impact of magnetic field strength on neutrino signals. In Section 4, we summarize the results.

2. WEAK INTERACTIONS IN STRONG MAGNETIC FIELD

2.1. Interaction cross section

The weak interaction Lagrangian reads (Weinberg 2005):

$$L_{\text{int}} = \frac{G_F \cos \theta_C}{\sqrt{2}} (N_\mu^\dagger L^\mu + N^\mu L_\mu^\dagger), \quad (1)$$

where $G_F = 1.166 \times 10^{-5} \text{GeV}^{-2}$ is the Fermi coupling constant, θ_C is the Cabbibo angle, for which we set the value $\cos^2(\theta_C) = 0.95$. L^μ and N_μ are the leptonic charged current and baryonic charged current. Hereafter, the reaction $\nu_e + n \rightarrow e^- + p$ is used to illustrate the impact of a magnetic field

on the cross-section. For this reaction, L^μ and N^μ is given by:

$$L^\mu = \bar{\psi}_e \gamma^\mu (1 - \gamma_5) \psi_\nu, \quad (2)$$

$$N^\mu = \bar{\psi}_n \gamma^\mu [g_V - g_A \gamma_5] \psi_p. \quad (3)$$

where ψ_e, ψ_ν are lepton fields and ψ_n and ψ_p are baryon fields, respectively. g_V and g_A are the form factors, and we set $g_V = 1$ and $g_A/g_V = 1.26$, respectively. γ_5 is the 5-th Dirac Matrices. The weak interaction is usually described by exchanging a W or Z boson, which has a mass smaller than 100 GeV. This work only considers magnetic field strength smaller than 10^{18} G, which cannot affect weak interaction Lagrangian. The interaction amplitude M is given by (Johnson & Lippmann 1949; Cheng et al. 1993; Reddy et al. 1998):

$$M = \frac{iG_F \cos \theta_C}{\sqrt{2}} [\bar{\psi}_p \gamma^\mu (g_V - g_A \gamma_5) \psi_n] [\bar{\psi}_e \gamma_\mu (1 - \gamma_5) \psi_\nu], \quad (4)$$

Under a strong magnetic field, one should expand the wave functions under cylindrical coordinates with z -axis chosen as the direction of the magnetic field (Johnson & Lippmann 1949; Delsante & Frankel 1978, 1980; Duan & Qian 2004, 2005):

$$\psi_{e^-} = \frac{e^{i[k_{ez}z - E_e t + (n_e - r_e)\phi]}}{\sqrt{2\pi L/eB}} U_{e^-}, \quad (5)$$

$$\psi_p = \frac{e^{i[k_{pz}z - E_p t + (r_p - n_p)\phi]}}{\sqrt{2\pi L/eB}} U_p, \quad (6)$$

$$\psi_n = \frac{e^{i(\mathbf{k}_n \cdot \mathbf{x} - E_n t)}}{L^{3/2}} U_n, \quad (7)$$

$$\psi_{\nu_e} = \frac{e^{i(\mathbf{k}_{\nu_e} \cdot \mathbf{x} - E_{\nu_e} t)}}{L^{3/2}} U_{\nu_e}, \quad (8)$$

where n_i is the n th Landau level of species i , U_i is the spinor of particles i , and k_{iz} is the z -axis momentum of particle i . Since the nuclear magneton is three orders of magnitude smaller than the Bohr magneton due to heavy nuclear mass, the magnetic effects on nucleons are ignored. Three active neutrinos are also free from the magnetic field effects. Therefore, both neutrons and neutrinos have isotropic momentum \mathbf{k}_n and \mathbf{k}_{ν_e} . The cross section is given by the integration of $d\sigma$, whose expression is (Peskin & Schroeder 1995):

$$d\sigma = \sum_{s_p} \sum_{s_e} \frac{L dk_{ez}}{(2\pi)} \frac{1}{2E_e 2E_p} \frac{L^3 d^3 k_p}{(2\pi)^3} \frac{|iM|^2}{2E_{\nu_e} 2E_n |v_{\nu_e} - v_n|} \times \\ (2\pi)^2 \delta(E_e + E_p - E_\nu - E_n) \delta(p_e + p_p - p_\nu - p_n). \quad (9)$$

We applied the results from Duan & Qian (2004, 2005) with the 0-th order of approximation:

$$\sigma_{\nu N}(E_n, B) = \sigma_B^1 \left[1 + 2\chi \frac{(f \pm g)g}{f^2 + 3g^2} \cos \Theta_\nu \right] + \\ \sigma_B^2 \left[\frac{f^2 - g^2}{f^2 + 3g^2} \cos \Theta_\nu + 2\chi \frac{(f \mp g)g}{f^2 + 3g^2} \right], \quad (10)$$

where we have

$$\sigma_B^1 = \frac{G_F^2 \cos^2 \theta_C}{2\pi} (f^2 + 3g^2) \times eB \sum_{n=0}^{n_{\max}} \sum_{s=-1}^{s=1} \frac{g_n E_n}{\sqrt{E_n^2 - m_e^2 - (2n + s - 1)eB}}, \quad (11)$$

and

$$\sigma_B^2 = \frac{G_F^2 \cos^2 \theta_C}{2\pi} (f^2 + 3g^2) eB \frac{E_n}{\sqrt{E_n^2 - m_e^2}}, \quad (12)$$

where E_n is given by

$$E_n^2 = p_z^2 + m_e^2 + (2n + s - 1)eB, \quad (13)$$

and n is the Landau quantum number (Landau & Lifshits 1991) and $s = \pm 1$ is the spin of electrons and positrons. In Eq. 10, Θ_ν is the angle between neutrino momentum and the magnetic field, the upper sign is for $\nu_e + n$ reaction, and the lower sign is for $\bar{\nu}_e + p$. In Duan & Qian (2005), higher-order terms are considered to correct the nucleus mass effect during interaction. However, we ignore this correction since it does not affect the cross-section significantly (see Fig. 3 of Duan & Qian (2005)). Several previous studies (Maruyama et al. 2022; Famiano et al. 2022, 2020; Luo et al. 2020) have also adopted the same approximation.

2.2. Chemical potential

Inside the magnetic field, electrons (positrons) obey the Fermi-Dirac distribution but with the Landau quantization of E_n as we mentioned above. The chemical potential μ_e is evaluated from the charge neutrality of plasma, i.e., the net number density of both electrons and positrons should be balanced with the ions, where N_A is the Avogadro number. For a magnetized plasma, the momentum space of electrons and positrons is quantized as

$$2 \frac{d^3 p}{(2\pi)^3} f_{\text{FD}}(E_e, \pm \mu_e; T) \rightarrow eB \sum_{n=0}^{\infty} (2 - \delta_{n0}) \frac{dp_z}{4\pi^2} f_{\text{FD}}(E_n, \pm \mu_e; T), \quad (14)$$

then, the net electron number density is given by

$$\begin{aligned} \rho N_A Y_e = n_e = & \frac{m_e \omega_c}{(2\pi)^2} \sum_0^{n_{\max}} \int d\mathbf{p} \left[f_{\text{FD}}(E_n, +\mu_e; T)_{s=-1} \right. \\ & + f_{\text{FD}}(E_n, +\mu_e; T)_{s=1} - f_{\text{FD}}(E_n, -\mu_e; T)_{s=-1} \\ & \left. - f_{\text{FD}}(E_n, -\mu_e; T)_{s=1} \right]. \end{aligned} \quad (15)$$

Here, $\omega_c = eB/m_e$ is the cyclotron frequency, and $s = \pm 1$ represents the spin state of electrons and positrons. Notice that inside the magnetic field, the spin is only parallel or anti-parallel with the magnetic field. For the plasma with known electron number density n_e , temperature T , and field strength B , this relation should provide the value of chemical potential. In the limit of $T \rightarrow 0$, all

electrons are degenerate (there are no positrons since their chemical potential is negative), and the number density is given by:

$$n_e = \frac{2m\omega_c}{(2\pi)^2} \left[(E_F^2 - m_e^2)^{1/2} + 2 \sum_{n=1}^{n_{\max}} \sqrt{E_F^2 - m_e^2 - 2neB} \right], \quad (16)$$

which is consistent with [Delsante & Frankel \(1980\)](#).

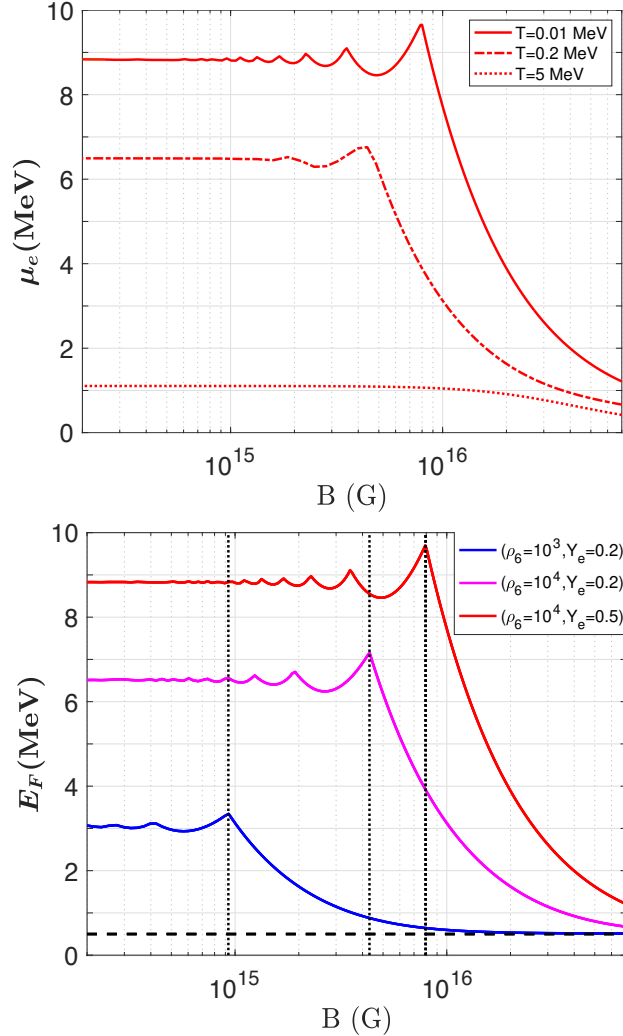


Figure 1. Upper panel: The chemical potential as a function of magnetic field strength for different temperatures, with $\rho = 10^{10} \text{ g cm}^{-3}$ and $Y_e = 0.5$. The solid line, dashed line and dotted line correspond to $T = 0.01 \text{ MeV}$, $T = 0.2 \text{ MeV}$ and $T = 5 \text{ MeV}$, respectively. The solid line is consistent with the red line on the lower panel since under this density and temperature, electrons are already in a degenerate state. Lower panel: Fermi energy E_F as a function of magnetic field strength with ρ_6, Y_e for different combinations as $(10^3, 0.2)$, $(10^4, 0.2)$ and $(10^4, 0.5)$, respectively. If the magnetic field is relatively weak, E_F becomes the same as a field-free case. On the other hand, E_F approaches $m_e = 0.511 \text{ MeV}$ (horizontal dashed line) when $B > B_{\text{crit}}$, vertical dotted lines represent the value of B_{crit} in each set of ρ and T .

The upper panel of Fig.1 shows chemical potential as a function of magnetic field strength at different temperatures. We set $\rho_6 \equiv \rho/10^6 \text{ g cm}^{-3} = 10^4$ and $Y_e = 0.5$ in this panel. In general,

chemical potential increases as temperature decreases (from dotted line to solid line in the upper panel of Fig. 1). While for an extremely low temperature, Eq. 15 will recover the degenerate case as Eq. 16, i.e., the red solid lines in both panels are identical to each other (temperature is set to be zero in the bottom panel of Fig. 1).

On the other hand, the chemical potential is reduced with increasing magnetic field strength. This is due to the extra energy contributed from the field to e^\pm . In the case of strong fields, e^\pm only occupy the lowest Landau level (LLL), so that μ_e decreases monotonically as a function of B , and approaches the asymptotic value m_e for an extremely strong magnetic field. In the case of degenerate plasma, the critical magnetic field strength B_{crit} for the scenario that only LLL is occupied reads

$$B_{\text{crit}} = \frac{\pi}{e} \left[2\pi(\rho Y_e)^2 \right]^{1/3}. \quad (17)$$

When the magnetic field strength is below B_{crit} , E_F shows a zig-zag pattern (bottom panel of Fig.1). The reason is as follows: for an extremely strong magnetic field, only the LLL is occupied. With decreasing magnetic field strength, the new Landau level pops up, and then, E_F decreases in order to cancel the extra energy that is carried by the magnetic field. The value of E_F again increases since the canceling effect decreases monotonically with decreasing magnetic field. Such a pattern will be repeated until the next Landau level pops up. For a weak magnetic field ($B < 10^{15}$ G), E_F values recover to the non-magnetized plasma cases: $E_F = 3.01$ MeV (blue line), 6.51 MeV (pink line), and 8.82 MeV (red line) for the (ρ_6, Y_e) combinations we chose.

3. THE NEUTRINO TRANSPORT INSIDE MAGNETIC FIELD

3.1. Method

Neutrino transport from opaque to transparent regions is among the most crucial and challenging parts to model, owing to the large variety of scales involved and the fine spatial resolutions needed to obtain accurate results. One efficient way to model the neutrino transport is the leakage scheme, which was first developed in the 1980s to solve the neutrino transport in CCSN at intermediate densities (van Riper & Lattimer 1981; Bruenn 1985; Burrows et al. 2000; Janka & Mueller 1996; Rosswog & Liebendoerfer 2003; Ruffert et al. 1996). The treatment of this regime is difficult since neither transparency nor opaque is a valid assumption. The leakage scheme describes the neutrino spectrum as a Fermi-Dirac distribution with a local chemical potential μ_{ν_i} for a neutrino species i . Neutrinos are approximately treated as they leak from the neutrino-sphere R_{ν_i} , which by definition is where the neutrino optical depth τ_{ν_i} equals to $2/3$ (this is similar to the definition of the photosphere of stars). One can calculate the optical depth from the integration of local opacity κ_{tot} , which is determined by the local mean free path of neutrinos or, equivalently, by the interaction rates of the neutrino processes (scattering, absorption, and emission). The total opacity κ_{tot} of electron type neutrinos are given by (Ruffert et al. 1996)

$$\kappa_{\text{tot},j}(\nu_e) = \kappa_{a,j}(\nu_e n) + \kappa_{s,j}(\nu_e n) + \kappa_{s,j}(\nu_e p) \quad (18)$$

$$\kappa_{\text{tot},j}(\bar{\nu}_e) = \kappa_{a,j}(\bar{\nu}_e p) + \kappa_{s,j}(\bar{\nu}_e n) + \kappa_{s,j}(\bar{\nu}_e p), \quad (19)$$

where a represents the absorption process and s stands for scattering process. Index j is introduced to denote the opacities for neutrino-number transport ($j = 0$) and neutrino-energy transport ($j = 1$),

respectively. As discussed in Sec. 2.1, inside a magnetic field, the absorption cross sections differ from the field-free case and the absorption opacities of ν_e and $\bar{\nu}_e$ read

$$\kappa_{a,j}^B(\nu_e n) = A\rho Y_{\text{np}} \times \frac{\int_0^\infty dE_{\nu_e} \sigma(E_n, B) E_{\nu_e}^{2+j} f_{\text{FD}}(E_{\nu_e}, \eta_{\nu_e}; T_{\nu_e}) g[E_n, \mu_e(B); T_e]}{\int_0^\infty dE_{\nu_e} E_{\nu_e}^{2+j} f_{\text{FD}}(E_{\nu_e}, \eta_{\nu_e}; T_{\nu_e})}, \quad (20)$$

$$\kappa_{a,j}^B(\bar{\nu}_e p) = A\rho Y_{\text{pn}} \times \frac{\int_0^\infty dE_{\bar{\nu}_e} \sigma(E_n, B) E_{\bar{\nu}_e}^{2+j} f_{\text{FD}}(E_{\bar{\nu}_e}, \eta_{\bar{\nu}_e}; T_{\bar{\nu}_e}) g[E_n, -\mu_e(B); T_e]}{\int_0^\infty dE_{\bar{\nu}_e} E_{\bar{\nu}_e}^{2+j} f_{\text{FD}}(E_{\bar{\nu}_e}, \eta_{\bar{\nu}_e}; T_{\bar{\nu}_e})}, \quad (21)$$

where $\eta_{\nu_e} = \mu_{\nu_e}/k_B T$ is the neutrino degeneracy parameter (same definition for $\eta_{\bar{\nu}_e}$), $\sigma(E_n, B)$ is taken from Eq. 10 and electron chemical potential $\mu_e(B)$ is calculated from Eq. 15. $g(E_n, \mu_e; T_e)$ is the Pauli blocking factor for Fermion. Y_{np} and Y_{pn} are coefficients that include the Pauli blocking effects in the phase space of neutrons and protons (See Appendix A for those expressions). Since the magnetic moment of nucleons is negligible due to their heavy mass, we ignore the impacts on neutrino scattering processes. One can find their expressions of the cross section and opacity in Ruffert et al. (1996). For heavy-lepton neutrinos (i.e., ν_τ and ν_μ), only scattering processes are included:

$$\kappa_{\text{tot},j}(\nu_x) = \kappa_{s,j}(\nu_x n) + \kappa_{s,j}(\nu_x p). \quad (22)$$

Finally, the optical depth is given by

$$\tau_{\nu_i,j}(r) = \int_r^\infty ds \kappa_{\text{tot},j}(\nu_i), \quad (23)$$

and neutrinosphere by definition, is given by $\tau_{\nu_i,j}(R_\nu) = 2/3$. Optical depth $\tau_{\nu_i,j}(r)$ describes the local neutrino mean free path. In the equilibrium-diffusive regime where $\tau \gg 1$ (densities $\rho > 10^{12} \text{ g cm}^{-3}$), neutrino-nucleon interaction is strong enough so that neutrinos are trapped, which means that the thermal and weak equilibrium holds. In contrast, for $\tau \ll 1$ ($\rho < 10^9 \text{ g cm}^{-3}$), matter can be treated as transparent to neutrinos due to the inefficient interaction rate, i.e., $\eta_{\nu_i}(r)$ vanished for such a free streaming region. It is worth mentioning that an advanced leakage schemes (Perego et al. 2016) consider the modification of neutrino spectrum $f_\nu = f_\nu^{tr} + \delta f_\nu$, which we do not include in this study.

This work applied the open-source GR1D code to simulate 1-D SNe explosion (O'Connor & Ott 2010; O'Connor 2015). We used the LS180 EOS (Lattimer & Swesty 1991) and took a $9.6 M_\odot$ progenitor model with zero metallicity from Heger (Private Communication). The collapse phase employs the parameterization scheme for electron captures following Liebendörfer (2005) and we switch to the leakage scheme after the core bounce, defined as the moment when entropy per baryon at the edge of the inner core reaches $3 k_B$. We modified the leakage scheme of neutrino transport in GR1D based on Eq. 20 and Eq. 21. We set a cut-off distance to be $r_{\text{cut}} = 100 \text{ km}$ and set magnetic field strength to be a constant value in the region $r < r_{\text{cut}}$ while there is no magnetic field for $r > r_{\text{cut}}$ in our CCSN

simulation¹. Although Eq. 10 shows the angle dependence of neutrino momentum with the magnetic field, the value of Θ_ν is fixed to 0 due to the limitation of 1D simulation. Further multi-dimensional simulation could be carried out based on the data we obtained.

3.2. Results

Fig. 2 illustrates the total opacity κ_{tot} of neutrinos (blue lines, left y -axis) and anti-neutrinos (red lines, right y -axis) during different stages (1 ms, 50 ms, and 100 ms after core bounce, respectively) of CCSN. Our calculation uses the opacity for neutrino-energy transport $\kappa_{\text{tot},1}(\nu_i)$ to determine the neutrinosphere. Here, in order to make a clear comparison of the impacts of magnetic field, we use the extracted density, temperature and Y_e profiles at a certain time step from GR1D to calculate the opacity in this environment and make the plot. In the inner region of CCSN, neutrino scattering contributes opacity the most, so the modification of absorption processes can be ignored.

At a very early phase after core bounce, shock propagates in high-density and high-temperature region, so the magnetic field does not make significant contributions, i.e., there is no difference between each line for various magnetic field strengths (upper panel of Fig. 2). Magnetic field enhances absorption opacity when shock propagates to $r \geq 30$ km (middle and lower panel of Fig. 2). This is mainly caused by two effects: 1) Magnetic field quantizes the phase space of e^\pm , with extra magnetic energy contribution, which enhances the neutrino-nucleon interaction rates. 2) The electron chemical potential μ_e is suppressed since only LLL is occupied, as we discussed in Sec. 2.2, leading to a larger value of blocking factor $g(E_n, -\mu_e; T_e)$ than $g(E_n, \mu_e; T_e)$. So the enhancement of $\bar{\nu}_e$ opacity is more significant than that of ν_e .

At a relatively later stage ($t \sim 100$ ms), the matter cools down and the magnetic field could enhance opacity by about 2-3 orders of magnitude in the region $100 \text{ km} < r < 1000 \text{ km}$ inside CCSN (lower panel of Fig. 2). However, optical depth in such a later phase is mainly determined by the opacity of the inner region ($r < 30$ km) due to the sharp decay of opacity with radius. Therefore, the neutrinosphere would eventually become indistinguishable from the field-free scenario (see Fig. 3 below).

The enhanced opacity enlarges the radius of neutrinosphere, which is shown in Fig. 3 where time evolution of neutrinosphere for ν_e and $\bar{\nu}_e$ are shown in the upper and lower panel, respectively. The radius of neutrinosphere is indistinguishable under different magnetic field cases at $t < 10$ ms after core bounce. After a few dozens ms, when shock propagates outside the high-density and high-temperature region, κ_{tot} increases and one can see the enlargement of neutrinosphere as expected. Usually, without a magnetic field, the radius of the neutrinosphere is larger than that of anti-neutrinos. This is because the proton abundance reduces after the shock passage, leading to a smaller value of absorption opacity κ_a . However, for a magnetic field as strong as 7×10^{16} G (i.e., blue lines), $R_{\bar{\nu}_e}$ becomes comparable with R_{ν_e} , this is consistent with the fact that magnetic field enlarges $\kappa_a(\bar{\nu}_e)$ more than $\kappa_a(\nu_e)$ as we discussed above.

¹ A more realistic feature is the dipole magnetic field. For simplicity, we only consider such constant field strengths in this study.

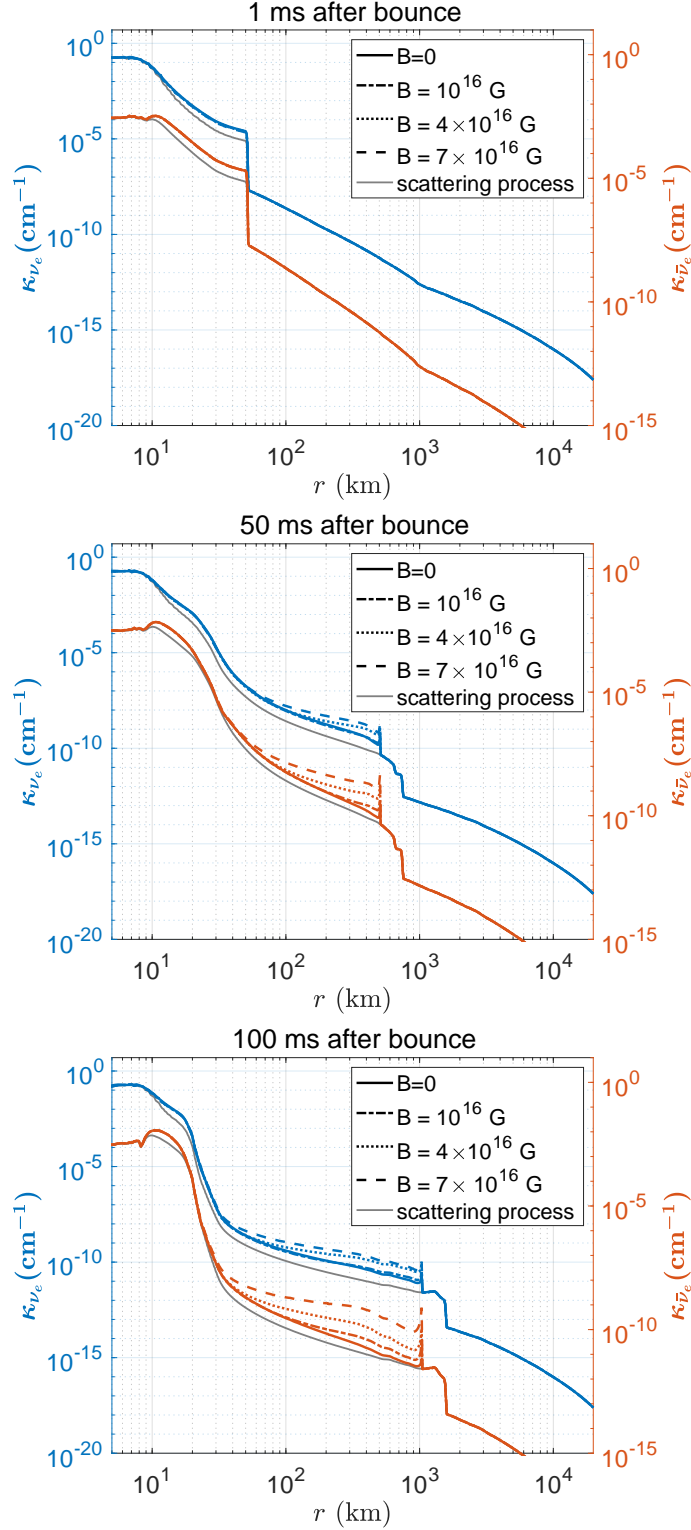


Figure 2. The opacity of $\nu_e, \bar{\nu}_e$ inside CCSN at different stages, i.e., 1 ms, 50 ms, and 100 ms after core bounce, separately. Blue lines are the opacity for ν_e , and red lines are for $\bar{\nu}_e$. The gray solid lines on all panels represent opacity contributed by scattering processes: $\nu_e + n(p) \rightarrow \nu_e + n(p)$ and $\bar{\nu}_e + n(p) \rightarrow \bar{\nu}_e + n(p)$. The line style, i.e., solid, dash-dotted, dotted, and dashed lines, represent the cases of $B = 0$, $B = 10^{16}$ G, $B = 4 \times 10^{16}$ G and $B = 7 \times 10^{16}$ G, respectively.

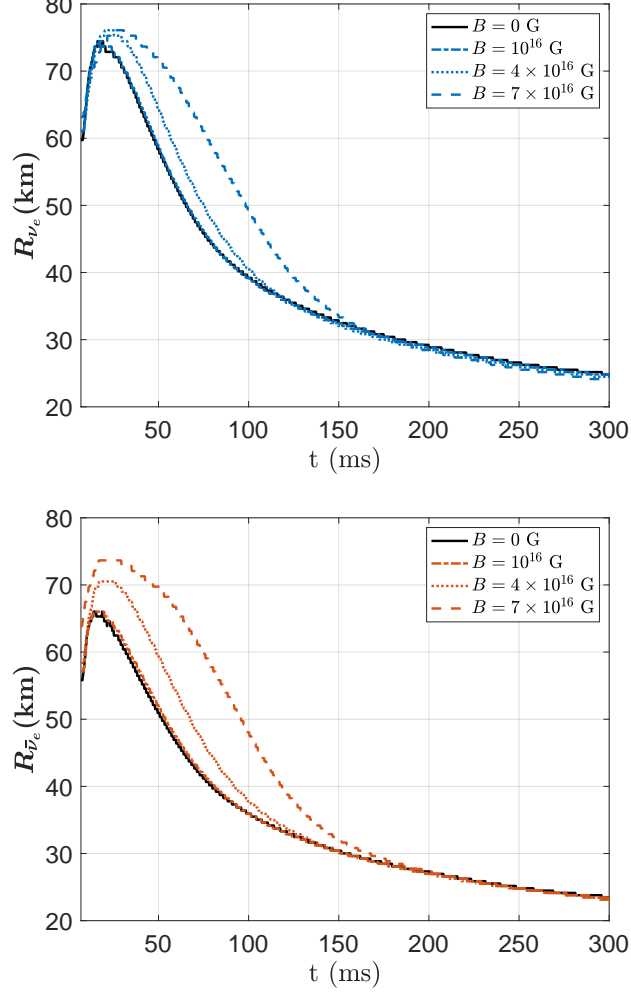


Figure 3. Upper panel: The neutrinosphere evolution (ν_e) after core bounce. Lower panel: The neutrinosphere evolution of $\bar{\nu}_e$ after core bounce. Black solid lines corresponding to the field free case; red, green, and blue lines corresponding to $B = 10^{16}$ G, $B = 4 \times 10^{16}$ G and $B = 7 \times 10^{16}$ G, respectively.

Neutrino emission is also important since it determines the neutrino luminosity. Under a magnetic field, local emission rates from electron (positron) capture are given by

$$R_{e,j}^B(e^- p) = A\rho Y_{\text{np}} \times \int_0^\infty dE_{\nu_e} \sigma(E_n, B) E_{\nu_e}^{2+j} g(E_{\nu_e}, \eta_{\nu_e}; T_{\nu_e}) f_{\text{FD}}[E_n, \mu_e(B); T_e], \quad (24)$$

$$R_{e,j}^B(e^+ n) = A\rho Y_{\text{pn}} \times \int_0^\infty dE_{\bar{\nu}_e} \sigma(E_n, B) E_{\bar{\nu}_e}^{2+j} g(E_{\bar{\nu}_e}, \eta_{\bar{\nu}_e}; T_{\bar{\nu}_e}) f_{\text{FD}}[E_n, -\mu_e(B); T_e], \quad (25)$$

where $j = 0$ is number emission rate, and $j = 1$ is energy emission rate. Pair creation ($e^- + e^+ \rightarrow \nu_e + \bar{\nu}_e$) and Bremsstrahlung effect are also included in GR1D code, we keep these two types of ν_e ($\bar{\nu}_e$) emission rates as field-free scenarios. Similar to [Rosswog & Liebendoerfer \(2003\)](#); [Ruffert et al.](#)

(1996), this work uses the effective emission rates in leakage scheme:

$$R_{\text{eff}} = \frac{R_{\text{emit}}}{1 + R_{\text{emit}}/R_{\text{diff}}}, \quad Q_{\text{eff}} = \frac{Q_{\text{emit}}}{1 + Q_{\text{emit}}/Q_{\text{diff}}}, \quad (26)$$

where R_{emit} and Q_{emit} are the local neutrino number and energy emission rates, respectively:

$$\begin{aligned} R_{\text{emit}} &= R_{e,0}^B + R_{\text{Pair}} + R_{\text{Brem}}, \\ Q_{\text{emit}} &= R_{e,1}^B + Q_{\text{Pair}} + Q_{\text{Brem}}. \end{aligned} \quad (27)$$

The local diffusion rates R_{diff} and Q_{diff} are calculated following the approximation made in [Rosswog & Liebendoerfer \(2003\)](#):

$$R_{\text{diff}} = \frac{4\pi c g_{\nu_i}}{(hc)^3} \frac{\zeta_{\nu_i}}{3\chi_{\nu_i}^2} T F_0(\eta_{\nu_i}), \quad (28)$$

$$Q_{\text{diff}} = \frac{4\pi c g_{\nu_i}}{(hc)^3} \frac{\zeta_{\nu_i}}{3\chi_{\nu_i}^2} T^2 F_1(\eta_{\nu_i}), \quad (29)$$

for neutrino species ν_i , where $\chi_{\nu_i} = \int \zeta_{\nu_i} dr$. The strong magnetic field changes the neutrino absorption rate on nucleons, i.e., value of $\zeta_{\nu_e}(\nu_e n)$ and $\zeta_{\bar{\nu}_e}(\bar{\nu}_e p)$ are modified. By definition, these two quantities are the local absorption rate over $\langle E^2 \rangle$ when calculating the diffusion rate:

$$\zeta_{\nu_e}(\nu_e n) = A\rho Y_{\text{np}} \times \quad (30)$$

$$\frac{\int_0^\infty \sigma(E_n, B) E_{\nu_e}^2 f_{\text{FD}}(E_{\nu_e}, \eta_{\nu_e}; T_{\nu_e}) g[E_n, \mu_e(B); T_e]}{\int_0^\infty E_{\nu}^4 f_{\text{FD}}(E_{\nu_e}, \eta_{\nu_e}; T_{\nu_e})},$$

$$\zeta_{\bar{\nu}_e}(\bar{\nu}_e p) = A\rho Y_{\text{np}} \times \quad (31)$$

$$\frac{\int_0^\infty \sigma(E_n, B) E_{\bar{\nu}_e}^2 f_{\text{FD}}(E_{\bar{\nu}_e}, \eta_{\bar{\nu}_e}; T_{\nu}) g[E_n, -\mu_e(B); T_e]}{\int_0^\infty E_{\bar{\nu}_e}^4 f_{\text{FD}}(E_{\bar{\nu}_e}, \eta_{\bar{\nu}_e}; T_{\bar{\nu}_e})}.$$

The effective neutrino emission rates Eq. 26 describes whether the neutrinos are diffused or emitted inside CCSN: for a high-density regime, diffusion rates are high, so it governs the main neutrino number and energy loss. In contrast, the main process becomes the local emission rate if neutrinos travel to a low-density region.

The effective energy emission rates are shown in Fig. 4 for different stages of CCSN (from up to bottom panel: 1 ms, 50 ms and 100 ms after the core bounce, respectively). Again, we compare the impacts of magnetic field under the extracted density, temperature and Y_e conditions in this figure. About 50 ms after core bounce (middle panel of Fig. 4), a magnetic field suppresses the effective neutrino emission rates in the range of $30 \text{ km} < r < 100 \text{ km}$, which is due to the enhancement of opacity we have shown in the middle panel of Fig. 2. Also, such a result is consistent with the reduction of the diffusion rates in this region (cf. Appendix B). At 100 ms after core bounce (lower panel of Fig. 4), shock has already propagated to the outer region, so the matter cools down and has a lower density. Diffusion is not essential in such an environment, while the local emission rates are enhanced more drastically (cf. Appendix B), leading to stronger effective emission rates.

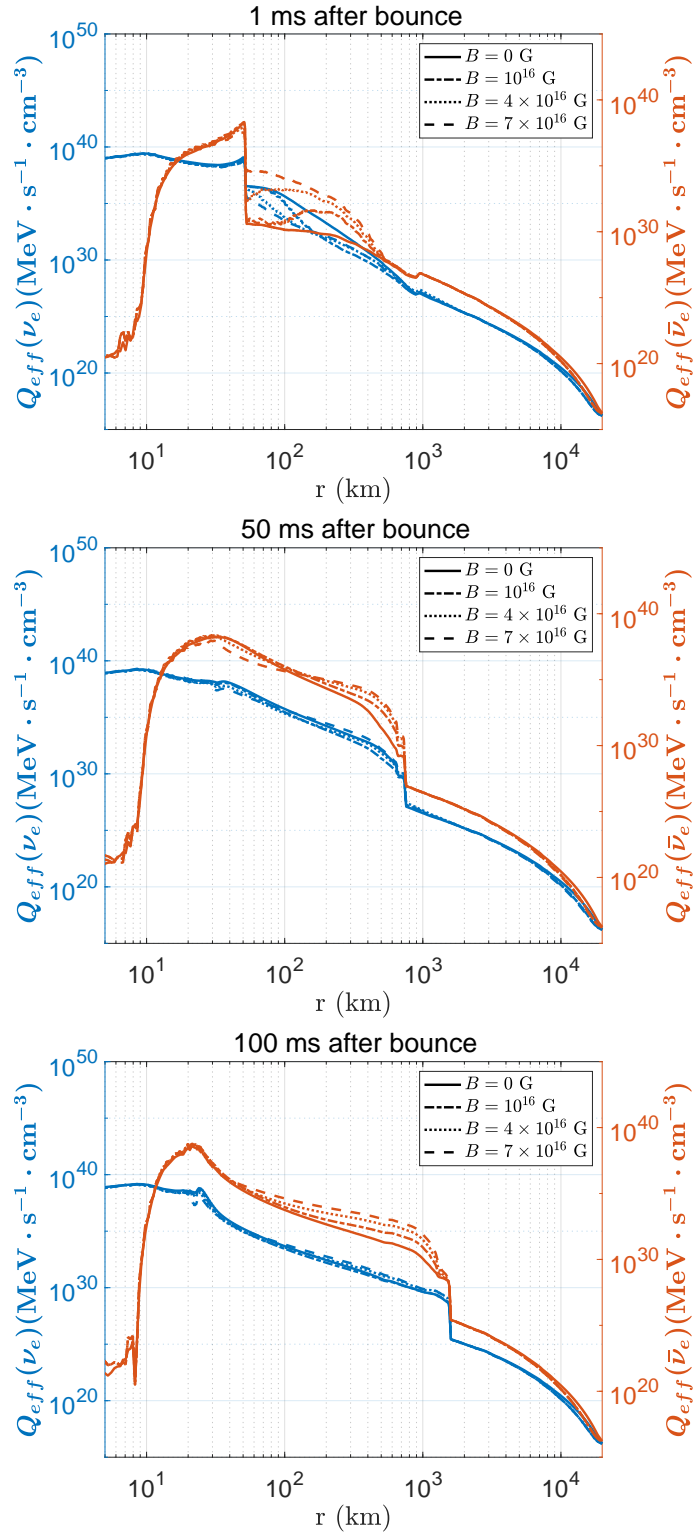


Figure 4. The effective energy emission rate of ν_e and $\bar{\nu}_e$ inside the CCSN after core bounce. The line-color convention follows Fig. 2.

The effective emission rates further determine neutrino luminosity, as shown in Fig. 5. After core bounce, ν_e is created by the electron capture on protons in the heated matter. A luminous flash of neutronization ν_e is radiated when shock travels to the low-density region outside the neutrinosphere. In field-free case, L_{ν_e} reaches the peak value near $4 \times 10^{53} \text{ erg} \cdot \text{s}^{-1}$ at $\sim 7 \text{ ms}$ (black solid line of the upper panel, also see the insert figure on the upper panel). The peak of $L_{\bar{\nu}_e}$ came shortly later than neutrinos (black solid line of the lower panel), with the value about $6 \times 10^{52} \text{ erg} \cdot \text{s}^{-1}$ at $\sim 30 \text{ ms}$; this is due to $\bar{\nu}_e$ production by pair process in shock-heated matter at a later time.

The situation changed after introducing the magnetic field: the peak luminosity decreases (red, green, and blue lines in each panel of Fig. 5). Especially, $L_{\bar{\nu}_e}$ peak value is more sensitive to the magnetic field. This is reasonable since in each panel of Fig.4, effective emission rates of $\bar{\nu}_e$ show more significant change than that of ν_e . More interestingly, since the magnetic field mainly enlarges the absorption rate of neutrinos, i.e. neutrinos spend more time trapped inside the neutrinosphere, therefore, after reaching the peak luminosity, both L_{ν_e} and $L_{\bar{\nu}_e}$ decay time scales become longer. Furthermore, the integrated energy of ν_e until 300 ms is reduced by about 10% ($1.13 \times 10^{52} \text{ erg}$ for field-free case, $1.03 \times 10^{52} \text{ erg}$ for a $7 \times 10^{16} \text{ G}$ magnetic field). While for $\bar{\nu}_e$, more trapping time leads to about 20% reduction of integrated energy ($6.92 \times 10^{51} \text{ erg}$ and $5.52 \times 10^{51} \text{ erg}$ for field-free and $7 \times 10^{16} \text{ G}$ cases, respectively).

Fig. 6 shows the time evolution of neutrino mean energies $\langle E_{\nu_e} \rangle$ (upper panel) and $\langle E_{\bar{\nu}_e} \rangle$ (lower panel) at the corresponding neutrinospheres. Because the employed leakage scheme assumes the neutrino energy spectra to be Fermi-Dirac, the neutrino mean energies are tightly correlated with the local matter temperatures. Thus the dependence of their time evolution on the magnetic field strength reflects the corresponding dependence of the neutrinosphere evolution (see Fig. 3). With a stronger magnetic field, the neutrino mean energies are smaller shortly after bounce and reach their peak values at later times. Note that this gray neutrino leakage scheme cannot accurately predict their energy spectra and mean values. Nevertheless, the general dependence on the magnetic field strength found here should still hold in simulations with more accurate multi-energy group neutrino transport.

We further inspect the impacts of the modified neutrino transport by magnetic field on the neutrino heating and explosion dynamics. Fig. 7 compares the evolution of the shock radius (R_{sh} , left y -axis) and gain radius (R_{g} , right y -axis) between the field-free and strongest field cases. The gain radius separates the net neutrino cooling and heating regions and its location and time evolution are crucial for the explodability of CCSNe. Before $\sim 75 \text{ ms}$ postbounce, R_{g} is smaller by at most $\sim 20 \text{ km}$ in the case of a strong magnetic field than that in the field-free case. Accordingly, the runaway shock expansion takes place earlier ($\sim 60 \text{ ms}$ postbounce) in the case of a strong magnetic field than in the field-free case ($\sim 120 \text{ ms}$ postbounce). During $\sim 75 - 100 \text{ ms}$, R_{g} in the case of a strong magnetic field becomes larger than in the field-free case due to the earlier runaway shock expansion. After $\sim 100 \text{ ms}$ postbounce, R_{g} is almost identical for the two cases because it has receded to below $\sim 50 \text{ km}$ where magnetic field does not affect the neutrino opacities (cf. Fig. 2) and transport (cf. Fig. 4). Our preliminary results suggest further efforts to investigate the impact of magnetic field on the CCSN neutrino transport and explosion dynamics with more accurate numerical schemes in realistic magnetohydrodynamic simulations.

4. DISCUSSIONS & CONCLUSION

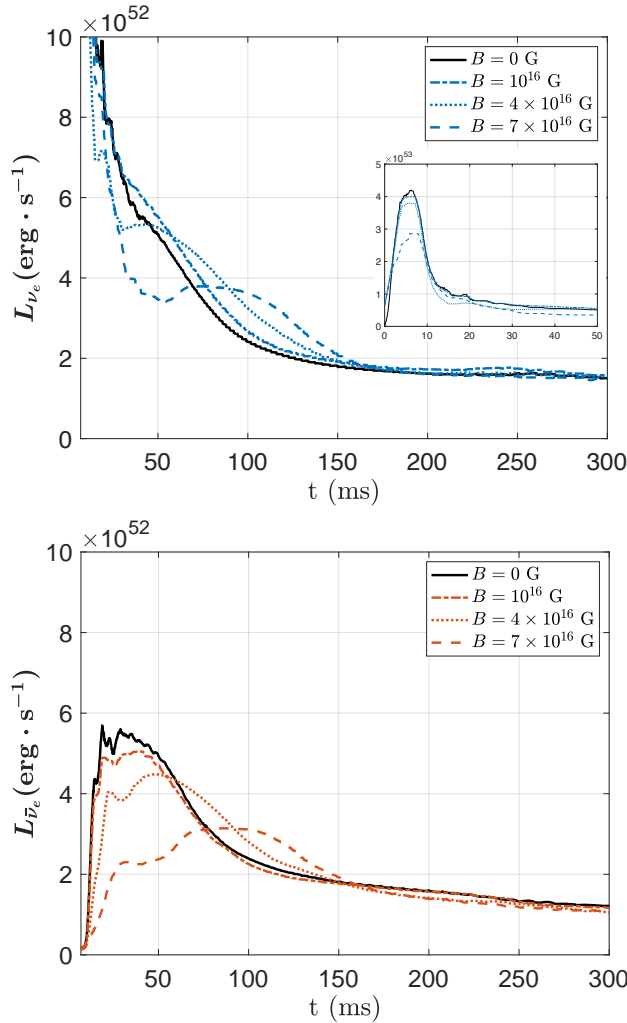


Figure 5. Upper panel: The neutrino luminosity (L_{ν_e}) after core bounce. Lower panel: The anti-neutrino luminosity ($L_{\bar{\nu}_e}$) after core bounce. The line-color convention follows Fig. 3.

In this study, we investigated the impacts of a strong magnetic field on the neutrino transport inside CCSN. The magnetic field affects the cross sections of the neutrino absorption and suppresses the chemical potential of the e^\pm since they only occupy the lowest Landau level under a strong magnetic field. We included these two major effects in the neutrino leakage scheme and employed the GR1D code to perform a 1-D CCSN simulation of a $9.6 M_\odot$ zero-metallicity progenitor. We assumed different magnetic field strengths ranging from 10^{16} G to 7×10^{16} G during the post-bounce phase. The magnetic field strength is restricted as a constant value inside $r < 100$ km of CCSN. As a result, the magnetic field enhances the absorption rates of the neutrino and anti-neutrons, leading to an enhancement of opacity and larger radii of the neutrinosphere (Fig. 2 and Fig. 3).

These effects make the trapping timescale of neutrinos inside the neutrinosphere longer, which results in a longer decay timescale of neutrino luminosities and a smaller peak neutrino luminosities (see Fig. 5). Accordingly, with a stronger magnetic field, the neutrino mean energies are smaller shortly after bounce and reach their peak values at later times (see Fig. 6). We tentatively found that a magnetic field results in a smaller gain radius at the time after early postbounce and thus

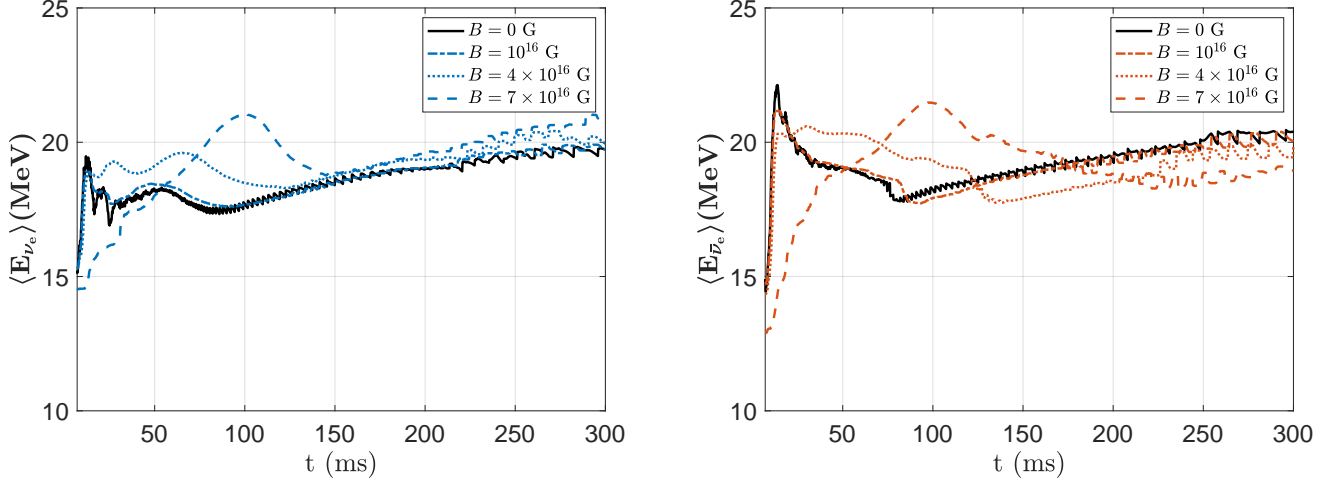


Figure 6. Upper panel: The neutrino mean energy ($\langle E_{\nu_e} \rangle$) as a function of time after core bounce. Lower panel: The anti-neutrino mean energy ($\langle E_{\bar{\nu}_e} \rangle$) as a function of time after core bounce. The line-color convention follows Fig. 3.

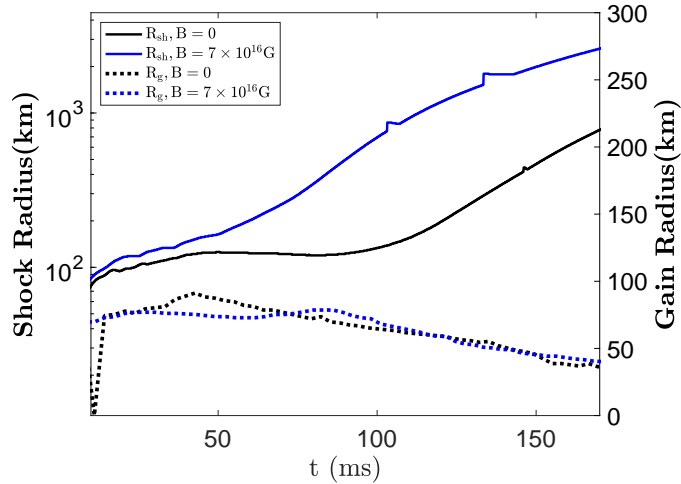


Figure 7. The comparison of shock radius R_{sh} (solid lines) and gain radius R_g (dotted lines) under field-free case (black lines) and 7×10^{16} G (blue lines). The gain radius separates the net neutrino cooling (below R_g) and heating (above R_g) regions.

an earlier runaway shock expansion. These findings stimulate future studies that incorporate more accurate neutrino transport schemes and realistic magnetohydrodynamic simulations to enhance the accuracy of the results.

Many physical processes, however, are not considered in this work due to the limitation of the 1-D simulation. Eq. 10 shows the Θ_ν dependence of the cross sections, so one should include the angle between the local neutrino momentum and the magnetic field in multi-dimensional simulations. We do apply the different Θ_ν to calculate the angle dependence of $\kappa_{abs}(\nu_e)$ as a function of η_{ν_e} . The results are shown in Fig. 8. Here, the width of blue and yellow bands are caused by changing the value of Θ_ν from 0 to π . The temperature and density are set to be $T = 1$ MeV and $\rho = 10^9$ g \cdot cm $^{-3}$.

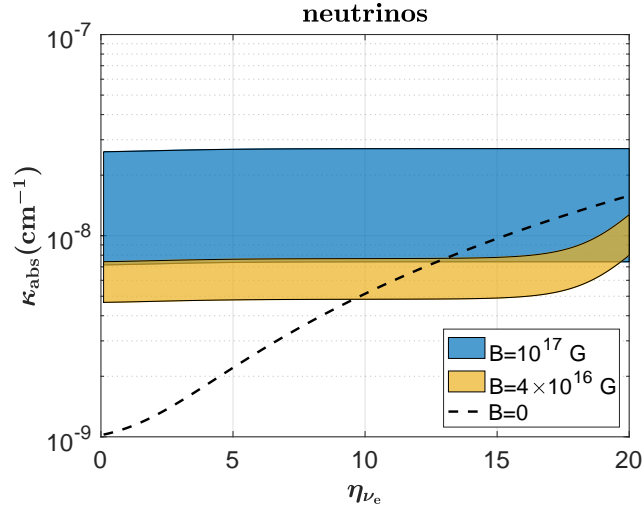


Figure 8. The neutrino absorption opacity κ_{abs} under different magnetic field strength. The black solid line is the field-free case, the blue band corresponds to 10^{17} G with different values of Θ_ν (the lower line of the band is the case that $\Theta_\nu = 0$, the upper line of the band is the case that $\Theta_\nu = \pi$), yellow band corresponds to 4×10^{16} G with the same meaning of the lower and upper lines. In this figure, $T = 1$ MeV and $\rho = 10^9 \text{ g} \cdot \text{cm}^{-3}$.

The absorption opacity can differ by a factor of 2 by changing the value of Θ_ν for $B = 10^{17}$ G. However, this is the upper limit of the magnetic field strength. The yellow band shows less than 20% difference for the case of a 4×10^{16} G magnetic field, indicating that neglecting the angular effect can be a reasonable approximation.

Moreover, the results we have shown in Fig. 3, Fig. 5, and Fig. 6 are based on the constant magnetic field inside $r < 100$ km region. We also set different r_{cut} values in the simulation, with the results of L_{ν_e} and $L_{\bar{\nu}_e}$ for different r_{cut} shown in Fig. 9. Noticeable differences still exist for the case in which the magnetic field is limited in $r < 70$ km. Nevertheless, the stellar magnetic field strength is proportional to R^{-3} in magneto-hydrodynamic simulations (see e.g., [Obergaullinger & Aloy 2021](#); [Powell et al. 2023](#)), so more realistic simulations with a dipole magnetic field should be carried out in the future. Recent studies [Betranhandy & O’Connor \(2020\)](#); [Guo et al. \(2024\)](#) showed that the neutrino pair production and neutrino-neutron scattering opacities can play an important role in the neutrino transport, which may also deviate in a strong magnetic field. As for multi-dimensional processes such as turbulence, there are recent works on effective modeling in 1-D SNe code ([Couch et al. 2019](#); [Müller 2019](#); [Mabanta et al. 2019](#)), which we plan to include in future studies.

In conclusion, the neutrino transport describes the absorption and scattering of neutrinos inside the central engines of CCSNe, and determines the energy spectra as well as luminosities of supernova neutrinos. Our results demonstrate the strong dependence of these properties against the magnetic field inside CCSN. Those quantities are crucial for the later nucleosynthesis, such as ν p-process, ν -process, and r -process. Therefore, our results indicate possible imprints of the magnetic field in the nucleosynthesis abundance pattern of the CCSN.

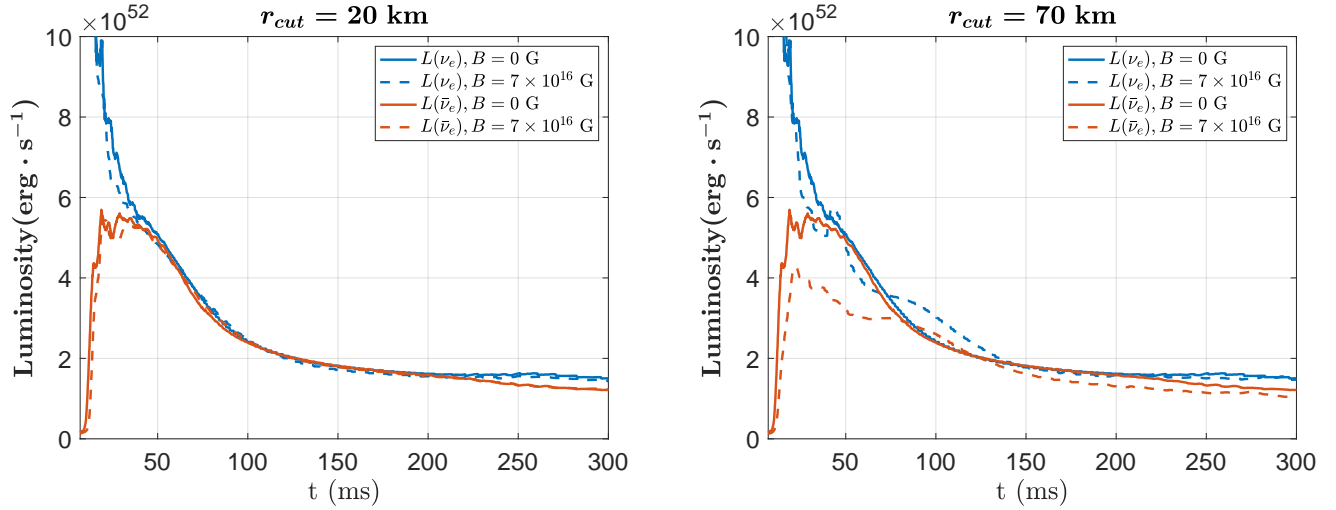


Figure 9. Upper panel: Luminosity for $r_{\text{cut}} = 20$ km. The solid lines represent the field-free case (blue for neutrinos and red for anti-neutrinos, respectively). The dashed lines represent the 7×10^{16} G case (blue for neutrinos and red for anti-neutrinos, respectively). Lower panel: Luminosity for $r_{\text{cut}} = 70$ km. The line-color convention is the same as the upper panel. For a small value of $r_{\text{cut}} = 20$ km, impacts of the magnetic field are barely seen, while the suppression on both L_{ν_e} and $L_{\bar{\nu}_e}$ are still observable if $r_{\text{cut}} = 70$ km.

- 1 We thank Motohiko Kusakabe, Ko Nakamura, Nobuya Nishimura, and Kanji Mori for their valuable
- 2 discussions. Y. Luo thanks the Institute of Modern Physics, Tsung-Dao Lee Institute at Shanghai
- 3 Jiao Tong University, and Nanjing University during his visits. Y. Luo is supported by the Boya
- 4 Fellowship of Peking University and the National Natural Science Foundation of China (NSFC,
- 5 No. 12335009). S. Zha is supported by the National Natural Science Foundation of China (NSFC,
- 6 Nos. 12288102, 12393811), the International Centre of Supernovae, Yunnan Key Laboratory (No.
- 7 202302AN360001) and the Natural Science Foundation of Yunnan Province (No. 202201BC070003)
- 8 and the Yunnan Fundamental Research Project (No. 202401BC070007). T. Kajino is supported in
- 9 part by the National Key R&D Program of China (2022YFA1602401), the National Natural Science
- 10 Foundation of China (No. 12335009), and Grants-in-Aid for Scientific Research of Japan Society for
- 11 the Promotion of Science (20K03958).

APPENDIX

A. FERMION BLOCKING EFFECTS OF NUCLEON

In Eq. 20 and Eq. 21, Y_{np} and Y_{pn} are given by (Ruffert et al. 1996; Rosswog & Liebendoerfer 2003):

$$Y_{np} = \frac{2Y_e - 1}{\exp(\eta_p - \eta_n) - 1}; Y_{pn} = \exp(\eta_p - \eta_n) \cdot Y_{np}, \quad (\text{A1})$$

where $\eta_{n(p)} = \mu_{n(p)}/k_B T$ is the degeneracy parameter of protons and neutrons. The neutrino degeneracy parameters η_ν are determined from local optical depth $\tau_{\nu_i}(r)$:

$$\begin{cases} \eta_{\nu_x}(r) = 0 \\ \eta_{\nu_e}(r) = \eta_{\nu_e}^{eq} \cdot [1 - \exp(-\tau_{\nu_e}(r))] \\ \eta_{\bar{\nu}_e}(r) = -\eta_{\nu_e}^{eq} \cdot [1 - \exp(-\tau_{\bar{\nu}_e}(r))] \end{cases} \quad (\text{A2})$$

Here, η^{eq} is the degeneracy parameter in the equilibrium state following the relation:

$$\eta_{\nu_e}^{eq} = -\eta_{\bar{\nu}_e}^{eq} = \eta_e(B) + \eta_p - \eta_n - Q/k_B T, \quad (\text{A3})$$

where $Q = m_n - m_p$.

B. LOCAL NEUTRINO DIFFUSION AND EMISSION RATES

Fig. 10 illustrates the local diffusion rate of neutrino.

Fig. 11 compares the local emission rate during different phases of CCSN.

REFERENCES

- Aglietta, M., et al. 1987, EPL, 3, 1315, doi: [10.1209/0295-5075/3/12/011](https://doi.org/10.1209/0295-5075/3/12/011)
- Arcones, A., & Thielemann, F.-K. 2023, Astron. Astrophys. Rev., 31, 1, doi: [10.1007/s00159-022-00146-x](https://doi.org/10.1007/s00159-022-00146-x)
- Arras, P., & Lai, D. 1999, Phys. Rev. D, 60, 043001, doi: [10.1103/PhysRevD.60.043001](https://doi.org/10.1103/PhysRevD.60.043001)
- Balasi, K. G., Langanke, K., & Martínez-Pinedo, G. 2015, Prog. Part. Nucl. Phys., 85, 33, doi: [10.1016/j.ppnp.2015.08.001](https://doi.org/10.1016/j.ppnp.2015.08.001)
- Bethe, H. A. 1990, Rev. Mod. Phys., 62, 801, doi: [10.1103/RevModPhys.62.801](https://doi.org/10.1103/RevModPhys.62.801)
- Betranhandy, A., & O'Connor, E. 2020, Phys. Rev. D, 102, 123015, doi: [10.1103/PhysRevD.102.123015](https://doi.org/10.1103/PhysRevD.102.123015)
- Bionta, R. M., et al. 1987, Phys. Rev. Lett., 58, 1494, doi: [10.1103/PhysRevLett.58.1494](https://doi.org/10.1103/PhysRevLett.58.1494)
- Bruenn, S. W. 1985, Astrophys. J. Suppl., 58, 771, doi: [10.1086/191056](https://doi.org/10.1086/191056)
- Burrows, A., Young, T., Pinto, P., Eastman, R., & Thompson, T. A. 2000, Astrophys. J., 539, 865, doi: [10.1086/309244](https://doi.org/10.1086/309244)
- Chakrabarty, S. 1996, Phys. Rev. D, 54, 1306, doi: [10.1103/PhysRevD.54.1306](https://doi.org/10.1103/PhysRevD.54.1306)
- Chakrabarty, S., Bandyopadhyay, D., & Pal, S. 1997, Phys. Rev. Lett., 78, 2898, doi: [10.1103/PhysRevLett.78.2898](https://doi.org/10.1103/PhysRevLett.78.2898)
- Cheng, B., Schramm, D. N., & Truran, J. W. 1993, Phys. Lett. B, 316, 521, doi: [10.1016/0370-2693\(93\)91038-O](https://doi.org/10.1016/0370-2693(93)91038-O)
- Couch, S. M., Warren, M. L., & O'Connor, E. P. 2019, doi: [10.3847/1538-4357/ab609e](https://doi.org/10.3847/1538-4357/ab609e)
- Delsante, A., & Frankel, N. 1978, Phys. Lett. A, 67, 279, doi: [10.1016/0375-9601\(78\)90303-1](https://doi.org/10.1016/0375-9601(78)90303-1)
- . 1980, Annals of Physics, 125, 135, doi: [https://doi.org/10.1016/0003-4916\(80\)90122-0](https://doi.org/10.1016/0003-4916(80)90122-0)
- Duan, H., & Qian, Y.-Z. 2004, Phys. Rev. D, 69, 123004, doi: [10.1103/PhysRevD.69.123004](https://doi.org/10.1103/PhysRevD.69.123004)

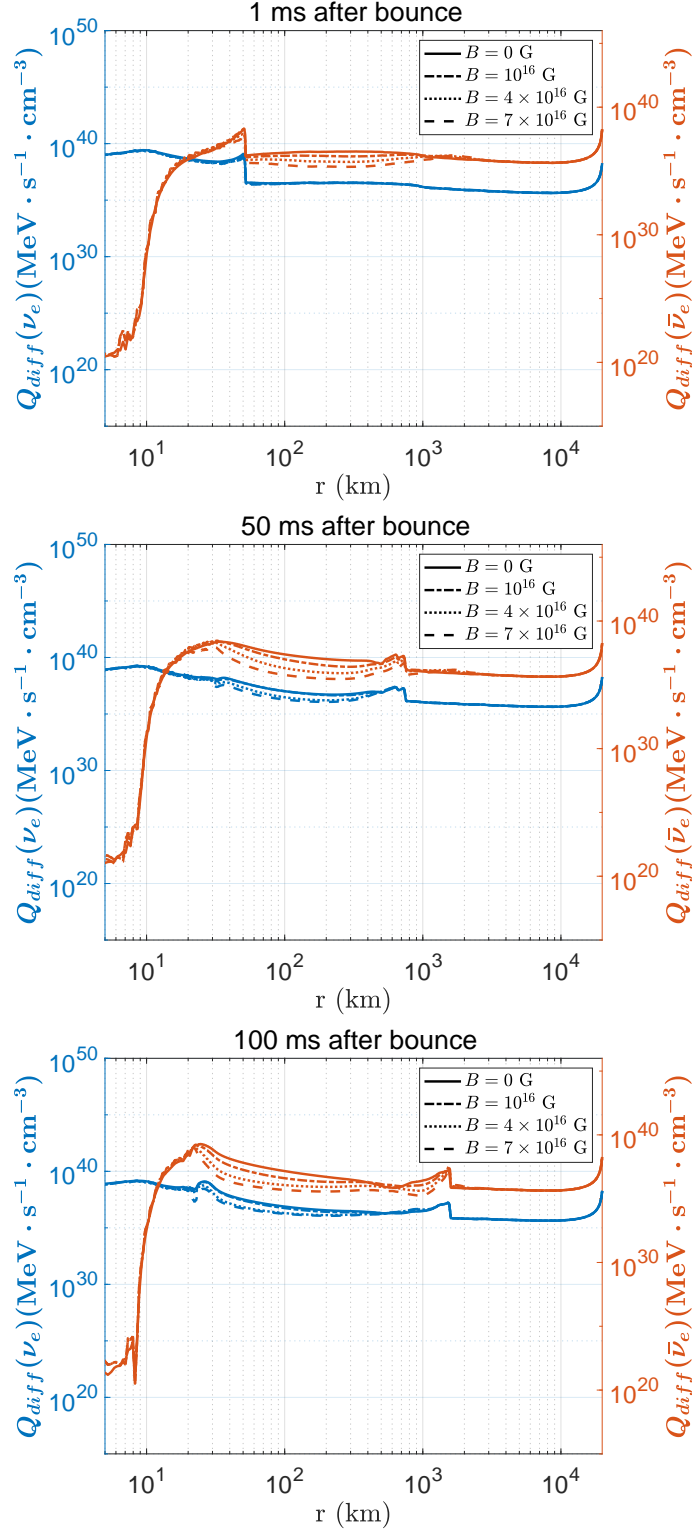


Figure 10. The diffusion rate of $\nu_e, \bar{\nu}_e$ inside the CCSN at different bouncing phases (1 ms, 50 ms and 100 ms, respectively). The blue lines are the emission rate for ν_e and the red lines are for $\bar{\nu}_e$. The results for the cases $B = 0$, $B = 10^{16}$ G, $B = 5 \times 10^{16}$ G and $B = 10^{17}$ G are shown in solid, dash-dotted, dotted, and dashed lines, respectively.

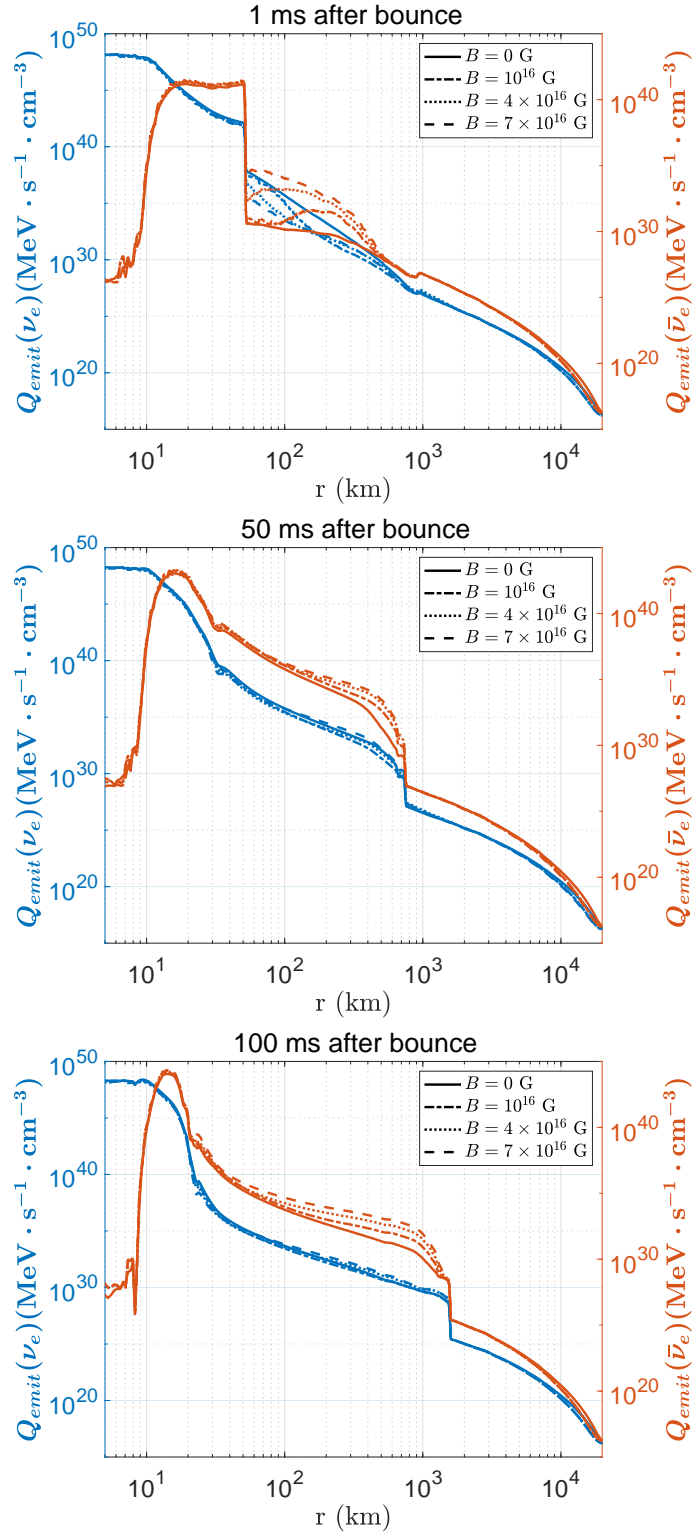


Figure 11. The emission rate of $\nu_e, \bar{\nu}_e$ inside the CCSN at different bouncing phases. The line-color convention follows Fig. 10.

- . 2005, *Phys. Rev. D*, 72, 023005, doi: [10.1103/PhysRevD.72.023005](https://doi.org/10.1103/PhysRevD.72.023005)
- Famiano, M., Balantekin, A. B., Kajino, T., et al. 2020, *Astrophys. J.*, 898, 163, doi: [10.3847/1538-4357/aba04d](https://doi.org/10.3847/1538-4357/aba04d)
- Famiano, M. A., Mathews, G., Balantekin, A. B., et al. 2022, *Astrophys. J.*, 940, 108, doi: [10.3847/1538-4357/ac9bf3](https://doi.org/10.3847/1538-4357/ac9bf3)
- Fischer, T., Whitehouse, S. C., Mezzacappa, A., Thielemann, F. K., & Liebendörfer, M. 2010, *A&A*, 517, A80, doi: [10.1051/0004-6361/200913106](https://doi.org/10.1051/0004-6361/200913106)
- Frohlich, C., Martinez-Pinedo, G., Liebendorfer, M., et al. 2006, *Phys. Rev. Lett.*, 96, 142502, doi: [10.1103/PhysRevLett.96.142502](https://doi.org/10.1103/PhysRevLett.96.142502)
- Guo, G., Martínez-Pinedo, G., & Wu, M.-R. 2024. <https://arxiv.org/abs/2401.10737>
- Hayakawa, T., Ko, H., Cheoun, M.-K., et al. 2018, *PhRvL*, 121, 102701, doi: [10.1103/PhysRevLett.121.102701](https://doi.org/10.1103/PhysRevLett.121.102701)
- Heger, A. Private Communication
- Heger, A., Kolbe, E., Haxton, W. C., et al. 2005, *Physics Letters B*, 606, 258, doi: [10.1016/j.physletb.2004.12.017](https://doi.org/10.1016/j.physletb.2004.12.017)
- Hirata, K., et al. 1987, *Phys. Rev. Lett.*, 58, 1490, doi: [10.1103/PhysRevLett.58.1490](https://doi.org/10.1103/PhysRevLett.58.1490)
- Janka, H. T. 2017, doi: [10.1007/978-3-319-21846-5_4](https://doi.org/10.1007/978-3-319-21846-5_4)
- Janka, H.-T., Langanke, K., Marek, A., Martinez-Pinedo, G., & Mueller, B. 2007, *Phys. Rept.*, 442, 38, doi: [10.1016/j.physrep.2007.02.002](https://doi.org/10.1016/j.physrep.2007.02.002)
- Janka, H. T., & Mueller, E. 1996, *Astron. Astrophys.*, 306, 167
- Johnson, M. H., & Lippmann, B. A. 1949, *Physical Review*, 76, 828, doi: [10.1103/PhysRev.76.828](https://doi.org/10.1103/PhysRev.76.828)
- Kajino, T., Mathews, G. J., & Hayakawa, T. 2014, *J. Phys. G*, 41, 044007, doi: [10.1088/0954-3899/41/4/044007](https://doi.org/10.1088/0954-3899/41/4/044007)
- Kitaura, F. S., Janka, H. T., & Hillebrandt, W. 2006, *A&A*, 450, 345, doi: [10.1051/0004-6361:20054703](https://doi.org/10.1051/0004-6361:20054703)
- Kiuchi, K., Cerdá-Durán, P., Kyutoku, K., Sekiguchi, Y., & Shibata, M. 2015, *Phys. Rev. D*, 92, 124034, doi: [10.1103/PhysRevD.92.124034](https://doi.org/10.1103/PhysRevD.92.124034)
- Kiuchi, K., Kyutoku, K., Sekiguchi, Y., Shibata, M., & Wada, T. 2014, *Phys. Rev. D*, 90, 041502, doi: [10.1103/PhysRevD.90.041502](https://doi.org/10.1103/PhysRevD.90.041502)
- Ko, H., et al. 2020, *Astrophys. J. Lett.*, 891, L24, doi: [10.3847/2041-8213/ab775b](https://doi.org/10.3847/2041-8213/ab775b)
- Ko, H., Jang, D., Cheoun, M.-K., et al. 2022, *ApJ*, 937, 116, doi: [10.3847/1538-4357/ac88cd](https://doi.org/10.3847/1538-4357/ac88cd)
- Kusakabe, M., Cheoun, M.-K., Kim, K. S., et al. 2019, *Astrophys. J.*, 872, 164, doi: [10.3847/1538-4357/aafc35](https://doi.org/10.3847/1538-4357/aafc35)
- Lai, D., & Qian, Y.-Z. 1998, *Astrophys. J.*, 505, 844, doi: [10.1086/306203](https://doi.org/10.1086/306203)
- Lai, D., & Shapiro, S. L. 1991, *ApJ*, 383, 745, doi: [10.1086/170831](https://doi.org/10.1086/170831)
- Landau, L. D., & Lifshits, E. M. 1991, *Course of Theoretical Physics, Vol. v.3, Quantum Mechanics: Non-Relativistic Theory* (Oxford: Butterworth-Heinemann)
- Langacker, P., Petcov, S. T., Steigman, G., & Toshev, S. 1987, *Nucl. Phys. B*, 282, 589, doi: [10.1016/0550-3213\(87\)90699-7](https://doi.org/10.1016/0550-3213(87)90699-7)
- Lattimer, J. M., & Swesty, F. D. 1991, *Nucl. Phys. A*, 535, 331, doi: [10.1016/0375-9474\(91\)90452-C](https://doi.org/10.1016/0375-9474(91)90452-C)
- Liebendörfer, M. 2005, *ApJ*, 633, 1042, doi: [10.1086/466517](https://doi.org/10.1086/466517)
- Luo, Y., Famiano, M. A., Kajino, T., Kusakabe, M., & Balantekin, A. B. 2020, *Phys. Rev. D*, 101, 083010, doi: [10.1103/PhysRevD.101.083010](https://doi.org/10.1103/PhysRevD.101.083010)
- Mabanta, Q. A., Murphy, J. W., & Dolence, J. C. 2019, *ApJ*, 887, 43, doi: [10.3847/1538-4357/ab4bcc](https://doi.org/10.3847/1538-4357/ab4bcc)
- Maruyama, T., Balantekin, A. B., Cheoung, M.-K., et al. 2022, *Phys. Lett. B*, 824, 136813, doi: [10.1016/j.physletb.2021.136813](https://doi.org/10.1016/j.physletb.2021.136813)
- Mikheev, S. P., & Smirnov, A. Y. 1986, *Nuovo Cim. C*, 9, 17, doi: [10.1007/BF02508049](https://doi.org/10.1007/BF02508049)
- Mösta, P., Ott, C. D., Radice, D., et al. 2015, *Nature*, 528, 376, doi: [10.1038/nature15755](https://doi.org/10.1038/nature15755)
- Mösta, P., Richers, S., Ott, C. D., et al. 2014, *Astrophys. J. Lett.*, 785, L29, doi: [10.1088/2041-8205/785/2/L29](https://doi.org/10.1088/2041-8205/785/2/L29)
- Müller, B. 2019, *MNRAS*, 487, 5304, doi: [10.1093/mnras/stz1594](https://doi.org/10.1093/mnras/stz1594)
- Nakamura, K., Kajino, T., Mathews, G. J., Sato, S., & Harikae, S. 2015, *Astron. Astrophys.*, 582, A34, doi: [10.1051/0004-6361/201526110](https://doi.org/10.1051/0004-6361/201526110)
- Nishimura, N., Takiwaki, T., & Thielemann, F. K. 2015, *Astrophys. J.*, 810, 109, doi: [10.1088/0004-637X/810/2/109](https://doi.org/10.1088/0004-637X/810/2/109)
- Obergaulinger, M., & Aloy, M.-A. 2021, *Mon. Not. Roy. Astron. Soc.*, 503, 4942, doi: [10.1093/mnras/stab295](https://doi.org/10.1093/mnras/stab295)

- O'Connor, E. 2015, *Astrophys. J. Suppl.*, 219, 24, doi: [10.1088/0067-0049/219/2/24](https://doi.org/10.1088/0067-0049/219/2/24)
- O'Connor, E., & Ott, C. D. 2010, *Class. Quant. Grav.*, 27, 114103, doi: [10.1088/0264-9381/27/11/114103](https://doi.org/10.1088/0264-9381/27/11/114103)
- O'Connor, E., & Ott, C. D. 2011, *ApJ*, 730, 70, doi: [10.1088/0004-637X/730/2/70](https://doi.org/10.1088/0004-637X/730/2/70)
- Oertel, M., Hempel, M., Klähn, T., & Typel, S. 2017, *Reviews of Modern Physics*, 89, 015007, doi: [10.1103/RevModPhys.89.015007](https://doi.org/10.1103/RevModPhys.89.015007)
- Perego, A., Cabezón, R., & Käppeli, R. 2016, *Astrophys. J. Suppl.*, 223, 22, doi: [10.3847/0067-0049/223/2/22](https://doi.org/10.3847/0067-0049/223/2/22)
- Peskin, M. E., & Schroeder, D. V. 1995, *An Introduction to quantum field theory* (Reading, USA: Addison-Wesley)
- Powell, J., Müller, B., Aguilera-Dena, D. R., & Langer, N. 2023, *MNRAS*, 522, 6070, doi: [10.1093/mnras/stad1292](https://doi.org/10.1093/mnras/stad1292)
- Price, D., & Rosswog, S. 2006, *Science*, 312, 719, doi: [10.1126/science.1125201](https://doi.org/10.1126/science.1125201)
- Radice, D., Burrows, A., Vartanyan, D., Skinner, M. A., & Dolence, J. C. 2017, *ApJ*, 850, 43, doi: [10.3847/1538-4357/aa92c5](https://doi.org/10.3847/1538-4357/aa92c5)
- Raynaud, R., Guilet, J., Janka, H.-T., & Gastine, T. 2020, *Sci. Adv.*, 6, eaay2732, doi: [10.1126/sciadv.aay2732](https://doi.org/10.1126/sciadv.aay2732)
- Reddy, S., Prakash, M., & Lattimer, J. M. 1998, *Phys. Rev. D*, 58, 013009, doi: [10.1103/PhysRevD.58.013009](https://doi.org/10.1103/PhysRevD.58.013009)
- Rosswog, S., & Liebendoerfer, M. 2003, *Mon. Not. Roy. Astron. Soc.*, 342, 673, doi: [10.1046/j.1365-8711.2003.06579.x](https://doi.org/10.1046/j.1365-8711.2003.06579.x)
- Roulet, E. 1991, *Phys. Rev. D*, 44, R935, doi: [10.1103/PhysRevD.44.R935](https://doi.org/10.1103/PhysRevD.44.R935)
- Ruffert, M. H., Janka, H. T., & Schaefer, G. 1996, *Astron. Astrophys.*, 311, 532, <https://arxiv.org/abs/astro-ph/9509006>
- Ruiz, M., Tsokaros, A., & Shapiro, S. L. 2020, *Phys. Rev. D*, 101, 064042, doi: [10.1103/PhysRevD.101.064042](https://doi.org/10.1103/PhysRevD.101.064042)
- Sasaki, H., Kajino, T., Takiwaki, T., et al. 2017, *Phys. Rev. D*, 96, 043013, doi: [10.1103/PhysRevD.96.043013](https://doi.org/10.1103/PhysRevD.96.043013)
- Sasaki, H., Takiwaki, T., Kawagoe, S., Horiuchi, S., & Ishidoshiro, K. 2020, *Phys. Rev. D*, 101, 063027, doi: [10.1103/PhysRevD.101.063027](https://doi.org/10.1103/PhysRevD.101.063027)
- Sumiyoshi, K., Yamada, S., Suzuki, H., & Chiba, S. 2006, *PhRvL*, 97, 091101, doi: [10.1103/PhysRevLett.97.091101](https://doi.org/10.1103/PhysRevLett.97.091101)
- Takiwaki, T., Kotake, K., & Sato, K. 2009, *Astrophys. J.*, 691, 1360, doi: [10.1088/0004-637X/691/2/1360](https://doi.org/10.1088/0004-637X/691/2/1360)
- Travaglio, C., Rauscher, T., Heger, A., Pignatari, M., & West, C. 2018, *ApJ*, 854, 18, doi: [10.3847/1538-4357/aaa4f7](https://doi.org/10.3847/1538-4357/aaa4f7)
- Valle, J. W. F. 1987, *Phys. Lett. B*, 199, 432, doi: [10.1016/0370-2693\(87\)90947-6](https://doi.org/10.1016/0370-2693(87)90947-6)
- van Riper, K. A., & Lattimer, J. M. 1981, *ApJ*, 249, 270, doi: [10.1086/159285](https://doi.org/10.1086/159285)
- Wanajo, S. 2006, *Astrophys. J.*, 647, 1323, doi: [10.1086/505483](https://doi.org/10.1086/505483)
- Wanajo, S., Janka, H.-T., & Kubono, S. 2011, *Astrophys. J.*, 729, 46, doi: [10.1088/0004-637X/729/1/46](https://doi.org/10.1088/0004-637X/729/1/46)
- Weinberg, S. 2005, *The Quantum theory of fields. Vol. 1: Foundations* (Cambridge University Press), doi: [10.1017/CBO9781139644167](https://doi.org/10.1017/CBO9781139644167)
- Woodsley, S. E., Hartmann, D. H., Hoffman, R. D., & Haxton, W. C. 1990, *Astrophys. J.*, 356, 272, doi: [10.1086/168839](https://doi.org/10.1086/168839)
- Woodsley, S. E., Heger, A., & Weaver, T. A. 2002, *Rev. Mod. Phys.*, 74, 1015, doi: [10.1103/RevModPhys.74.1015](https://doi.org/10.1103/RevModPhys.74.1015)
- Woodsley, S. E., Wilson, J. R., Mathews, G. J., Hoffman, R. D., & Meyer, B. S. 1994, *ApJ*, 433, 229, doi: [10.1086/174638](https://doi.org/10.1086/174638)
- Yoshida, T., Suzuki, T., Chiba, S., et al. 2008, *Astrophys. J.*, 686, 448, doi: [10.1086/591266](https://doi.org/10.1086/591266)